Metabolic and behavioral alterations associated with viral vector-mediated toxicity in the paraventricular hypothalamic nucleus

Rohan Savani[1,2], Erin Park[1,2], Nidhi Busannagari[1,2], Yi Lu[1], Hyokjoon Kwon[3], Le Wang[1, *], Zhiping P. Pang[1, *]

[1]The Child Health Institute of New Jersey, Robert Wood Johnson Medical School, Rutgers, The State University of New Jersey, New Brunswick, NJ, USA
[2]Department of Cell Biology and Neuroscience, Undergraduate Program, Rutgers, The State University of New Jersey, New Brunswick, NJ, USA
[3]Department of Medicine, Rutgers-Robert Wood Johnson Medical School, New Brunswick, NJ, 08901, USA

Main text Words: 4002

Figures: 4

*Corresponding authors:

Le Wang: lw611@rwjms.rutgers.edu

Zhiping P. Pang: pangzh@rwjms.rutgers.edu

ABSTRACT

Objective: Combining adeno-associated virus (AAV)-mediated expression of Cre recombinase with genetically modified floxed animals is a powerful approach for assaying the functional role of genes in regulating behavior and metabolism. Extensive research in diverse cell types and tissues using AAV-Cre has shown it can save time and avoid developmental compensation as compared to using Cre driver mouse line crossings. We initially sought to study the impact of ablation of corticotropin-releasing hormone (CRH) in the paraventricular hypothalamic nucleus (PVN) using intracranial AAV-Cre injection in adult animals.

Methods: In this study, we stereotactically injected AAV8-hSyn-Cre or a control AAV8-hSyn-GFP both Crh-floxed and wild-type mouse PVN to assess behavioral and metabolic impacts. We then used immunohistochemical markers to systematically evaluate the density of hypothalamic peptidergic neurons and glial cells.

Results: We found that delivery of one specific preparation of AAV8-hSyn-Cre in the PVN led to the development of obesity, hyperphagia, and anxiety-like behaviors. This effect occurred independent of sex and in both floxed and wild-type mice. We subsequently found that AAV8-hSyn-Cre led to neuronal cell death and gliosis at the site of viral vector injections. These behavioral and metabolic deficits were dependent on injection into the PVN. An alternatively sourced AAV-Cre did not reproduce the same results.

Conclusions: Our findings reveal that delivery of a specific batch of AAV-Cre could lead to cellular toxicity and lesions in the PVN that cause robust metabolic and behavioral impacts. These alterations can complicate the interpretation of Cre-mediated gene knockout and highlight the need for rigorous controls.

Keywords: AAV, toxicity, paraventricular hypothalamus, obesity

Introduction

Located in the ventral forebrain, the paraventricular nucleus of the hypothalamus (PVN) acts as a major integrative center for diverse regulatory functions, including neuroendocrine response, autonomic tone, and complex behaviors including food intake and social interaction [1, 2, 3]. Dissecting the molecular, morphological, and functional heterogeneity of the PVN has thus far given rise to several distinct cell types involved in the control of these processes.

Refining our understanding of how the PVN integrates and outputs multimodal information across neuroendocrine and autonomic pathways may inform several disorders, including cardiovascular, metabolic, and neuropsychiatric disorders [2, 4, 5]. However, the PVN contains spatially intermingled but functionally distinct populations that can only be selectively targeted through genetic access, such as conditional knockout (KO) by Cre-lox recombination [6, 7]. While much work relies on promoter-driven Cre expression, another standard method relies on adeno-associated virus-mediated Cre expression (AAV-Cre) [8, 9, 10, 11]. Methods such as AAV-mediated Cre delivery in adult mice are valuable approaches to bypass transient developmental transcription and ensure high-fidelity expression in specific brain regions [8, 12]. However, emerging evidence suggests that there may be deleterious effects associated with AAV-Cre, resulting in morphological and behavioral abnormalities even in the absence of loxP sequences [13, 14].

In this study, we assessed the striking phenotype that emerged from the delivery of an AAV-Cre-prepared virus in the PVN of adult homozygous floxed corticotropin-releasing hormone (*Crh*$^{f/f}$) mice. PVN CRH neurons are tightly linked to energy homeostasis—they respond to food cues, and acute manipulations decrease motivation to seek and consume food [8, 15, 16]. Chronic manipulations have been shown to confer risk to diet-induced weight gain, as well [17]. While knockout of CRH has not been shown to contribute to changes in metabolism or food intake thus far, these methods have used Cre driver lines or homologous recombination in embryonic stem cells [18, 19, 20]. As has been suggested for discrepancies in findings using knockout models of the type-1 CRH receptor, we hypothesized that developmental compensation may mask the metabolic effects of CRH knockout [21, 22]. We found that *Crh*$^{f/f}$ mice with putatively knocked out corticotropin-releasing hormone (CRH) via AAV-mediated expression of Cre recombinase in the PVN rapidly developed obesity and metabolic syndrome, which was an intriguing and unexpected finding. However, subsequent analyses for validation revealed that both CRH- and oxytocin-expressing neuron densities significantly decreased, likely due to

81 cellular toxicity at the injection sites. Our study confirms the importance of the PVN in the control
82 of metabolism and highlights the potential for toxicity due to a batch of a commonly used AAV,
83 which necessitates careful interpretation and proper controls for experiments utilizing viral
84 vectors.

85 **Hypothesis**

86 We hypothesize that the targeted disruption of corticotropin-releasing hormone (CRH)
87 expression within the paraventricular hypothalamic nucleus (PVN) through intracranial AAV8-
88 hSyn-Cre injection in adult animals may result in obesity and metabolic alterations.

89 **Methods**

90 ***Animals***
91 All experiments involving animals were conducted at the Child Institute of New Jersey, Rutgers
92 University, USA. All protocols involving mice were approved by the Rutgers University
93 Institutional Animal Care and Use Committee (IACUC) (Protocol # PROTO201702609) and by
94 the National Institute of Health (NIH) guidelines. The animals used in this study were 5-7 weeks
95 old at the time of stereotactic surgery. Homozygous *Crh*$^{f/f}$ mice (gift from Dr. Larry Zweifel) [23],
96 *Glp1r*$^{f/f}$ mice [24], and wild-type (C57BL/6) mice were used in this study. For surgical injections,
97 mice were anesthetized with isoflurane. For histological studies, mice were anesthetized with
98 isoflurane and then followed by transcardial perfusion. For each experimental paradigm,
99 littermate mice were randomized to each experimental group on the basis of body weight. Both
100 males and females were used in this study. Mice of both groups were housed together.
101 Investigators were blinded to treatment. The sample size required (n=5-7) for each group was
102 estimated from previous studies [18].

103 ***AAV vectors and stereotactic surgery***
104 The AAVs used in this study included pAAV-hSyn-EGFP (Addgene, #50465-AAV8, titer: titer
105 7×10^{12} vg/mL), pENN.AAV.hSyn.HI. eGFP-Cre.WPRE.SV40 (Addgene, #105540-AAV8, lot:
106 v107437, titer: $1\text{x}10^{13}$ vg/mL), and AAV-hSyn-GFP-Cre (UNC Viral Vector Core, AAV8, lot:
107 AV5053E, titer: $2.5 \text{ x } 10^{12}$ vg/mL). For stereotactic injections, mice were anesthetized with
108 isoflurane and placed in a stereotactic frame. Burr holes were drilled above the injection sites.
109 150 nL of the viruses were bilaterally stereotactically injected in the PVN (AP: -0.7, ML: ±0.18,
110 DV: -4.7) at a rate of 1 nL/s (eGFP for control group, Cre for experimental group). For
111 experiments in the dorsolateral septum (dLS), 100 nL of viruses were bilaterally injected in the

112 dLS (AP: +0.5, ML: ±0.45, DV: -2.7) at a rate of 1 nL/second. Mice recovered for at least 3
113 weeks prior to conducting behavioral experiments. Injection sites were confirmed by *post hoc*
114 histological examinations.

115 ***Metabolic phenotyping***

116 All experiments were conducted during the light cycle unless otherwise stated. Investigators
117 were blinded to conditions during experiments.

118 *Plasma corticosterone measurements*: Blood was collected either at the beginning of the ITT
119 test or during transcardiac perfusion. At least 10 µL was collected into EDTA-coated tubes and
120 then centrifuged at 8000rpm at 4°C for 5 minutes. Extracted plasma was stored at -80° C until
121 further processing. Corticosterone measurements were obtained with an ELISA as per
122 manufacturer's instructions (Enzo Life Sciences, ADI-900-097).

123 *Food intake*: Mice were singly housed before the experiment with ad libitum access to normal
124 chow (Purina Mouse Diet 5058) and water. Chow remaining in the cage after each day (12 hr.
125 light/dark cycle) was measured for 5 days and averaged together.

126 *EchoMRI/fat mass measurements*: Whole body composition and fat mass was measured by
127 EchoMRI (Echo Medical Systems, Houston, Texas).

128 *Comprehensive Lab Animal Monitoring System (CLAMS) assays*: *Crh*$^{f/f}$ mice were placed into
129 metabolic phenotyping cages (Columbus Instruments, OH, USA). Data was recorded every 15
130 minutes. Data was collected for 3 days (both light and dark cycles) after 2 days of habituation to
131 single housing within the cages.

132 *Glucose tolerance test (GTT) and insulin tolerance test (ITT)*: Mice were fasted overnight (GTT)
133 or for 6 hours (ITT). To minimize stress, 0.5 grams of chow was provided. For GTT, mice were
134 intraperitoneally (IP) administered 20% glucose. Blood glucose measurements were collected at
135 the 0, 15-, 30-, 60-, and 120-minute time points. For ITT, mice were IP-administered insulin.
136 Injection volumes were 0.1 mL/10 g body weight. Blood glucose measurements were collected
137 at the 0-, 15-, 30-, and 60-minute time points.

138 ***Behavioral assays***

139 *Open field test*: Mice were placed in the middle of a custom-made 45 x 45 cm square open field
140 arena for 10 minutes. Analysis was performed using DeepLabCut v2.2 [25]. We labeled 150-200
141 frames taken from 14 or 10 videos, as resolution changed between recording sessions (95% of

142 frames were used for training, 5% for testing). We used a ResNet50-based network with default
143 parameters for 225,000 or 450,000 training iterations (until loss plateaued). After analyzing
144 open-field videos, we then calculated the time spent in the inner zone (inner 3/5 of the arena,
145 ~25x25cm) using a region of interest tool. Distance traveled was calculated with custom code.
146 Investigators were blinded to the condition during analysis.

147 *Light-dark box test*: Mice were placed in the SmartCage system (AfaSci) light side of a
148 commercial light-dark box apparatus consisting of one dark and one illuminated compartment
149 connected by a door. Time spent in each zone, latency to enter the dark zone, and number of
150 entries were measured for 10 minutes. Data were analyzed using Excel.

151 ***Histology and immunohistochemistry (IHC) analysis***

152 Mice used for IHC analysis of CRH and oxytocin (OXT) were intracerebroventricularly
153 administered colchicine a day prior to perfusion. Mice were anesthetized with isoflurane and
154 perfused with PBS (pH 7.4) and then 4% paraformaldehyde (PFA). Coronal brain slices were
155 cryosectioned (50 μm). For IHC analyses, brain slices were first incubated in blocking buffer
156 (4% BSA, 1% goat serum in PBS) for 1 hour, then in primary antibody overnight at 4°C. Slices
157 were washed with blocking buffer 3x15 min prior to incubation with a secondary antibody at RT
158 for 2 hours, followed by further washing with PBS. Sections were mounted with Fluoroshield
159 with DAPI (Sigma-Aldrich, # F6057). Images were collected with a Zeiss LSM700 confocal
160 microscope. A Z-stack captured the entire thickness of the section with fluorescence. NeuN-
161 stained slices were imaged at a 5 μm-thickness interval for a total range of 25 μm. Imaging
162 analysis was performed using NIH-ImageJ and with the Allen Brain Atlas as a reference. The
163 number of OXT- and CRH-cells in the PVN was counted with the Cell Counter plugin. To
164 quantify NeuN density, images were background subtracted (20-pixel radius) before converting
165 to a binary image. Then, segmented particles were filtered by despeckling twice and watershed
166 transforming, followed by final counting (minimum size of 7 μm^2). GFAP and Iba1 fluorescence
167 area was calculated by dividing the area of thresholded signal by total PVN area. The
168 quantifications were performed by two independent investigators who were blinded to the
169 condition during analysis.

170 ***Antibodies***

171 The primary antibodies used in this study were rabbit Anti-CRH (1:500, BMA Biomedicals, #T-
172 4037, RRID: AB_2314240), mouse Anti-OXT (1:500 Sigma-Aldrich, #MABN844), rabbit Anti-

173 NeuN (1:500, Millipore, #ABN78, RRID: AB_10807945), rabbit Anti-GFAP (1:1000, Dako,
174 #Z0334, RRID: AB_10013382), and chicken Anti-Iba1 (1:500, Aves Labs, #IBA1-0020).

175 ***Statistical analysis***

176 Statistical analyses were performed using GraphPad Prism 9. Data were analyzed using
177 Student's two-tailed t-tests and two-way ANOVA followed by Bonferroni's multiple comparisons
178 tests. Data are presented as mean ± SEM. A p-value < 0.05 was considered statistically
179 significant.

180 **Results**

181 ***Delivery of AAV-mediated Cre in the PVN rapidly induces behavioral changes and***
182 ***metabolic syndrome in male Crh$^{f/f}$ mice.***

183 Our initial goal was to apprise the functional role of CRH by knocking it out in the PVN in adult
184 animals. To this end, we bilaterally stereotactically injected AAV8-hSyn-eGFP-Cre in the PVN of
185 5-7-week-old *Crh$^{f/f}$* mice, with AAV-hSyn-eGFP (Control) injected in littermate controls (**Fig. 1A**).
186 After four weeks of recovery, we found that plasma corticosterone levels in Cre-injected *Crh$^{f/f}$*
187 mice were markedly reduced, which was highly suggestive of possible loss of function of CRH
188 (**Fig. 1B**). Even with normal chow feeding, the Cre-injected mice showed robust and rapid body
189 weight gain within days. Cre-injected mice reached an average of 50.5 ± 0.7 grams in 6 weeks,
190 while the average body weight of control animals was 28.2 ± 0.7 grams (**Fig. 1C**). The
191 increased body weight in the Cre-injected group might be, at least in part, due to elevated food
192 intake (**Fig. 1D**). We repeated these experiments in an independent cohort of *Crh$^{f/f}$* female mice
193 (**Fig. S1A**). In this, the Cre-injected group fed with normal chow weighed 45.2 ± 4.2 grams 6
194 weeks after viral injection (**Fig. S1B**), indicating that the changes observed thus far occur in a
195 sex-independent manner.

196 As PVN-derived CRH is known to be involved in stress-related behaviors, coping, and relief [16,
197 26, 27, 28], we hypothesized that reduced CRH release and corticosterone levels (**Fig. 1B**) in
198 the Cre-injected animals would be anxiolytic. To test this hypothesis, we examined anxiety-like
199 behavior in AAV-Cre injected *Crh$^{f/f}$* male mice in the open-field and light-dark box assays (**Fig.**
200 **S2**). Contrary to what we hypothesized, we found that the Cre-injected mice spent less time in
201 the center zone in the open-field assay (**Fig. S2B**), and they spent more time in the dark zone
202 during the light-dark box test (**Fig. S2D**). These tests suggested that AAV-Cre in the adult PVN
203 may lead to heightened anxiety-like behaviors.

204 Nevertheless, the drastic increase in body weight of AAV-Cre-injected animals prompted us to
205 further assess their metabolic phenotype. We used CLAMS to measure energy intake and
206 expenditure, as well as to identify any changes in nutrient utilization. Compared to AAV-GFP-
207 injected animals, AAV-Cre-injected mice consumed less oxygen throughout the entire day (**Fig.**
208 **1E-F**). The respiratory exchange ratio was equal between both groups, indicating no shift in
209 nutrient utilization accompanying increases in weight (**Fig. 1G**). Energy expenditure was
210 significantly decreased in AAV-Cre-injected mice in both light and dark cycles (**Fig. 1H**). This
211 may be in part due to a decrease in locomotor activity (**Fig. 1I**). These data suggest that
212 alterations in energy expenditure may contribute to the development of obesity alongside
213 hyperphagia in AAV-Cre-injected mice. Consistent with these findings, Cre-injected mice display
214 significantly increased body fat composition (**Fig. 1J**) and significantly increased fasting plasma
215 glucose levels measured (**Fig. 1K**). To evaluate any changes in glucose and insulin
216 homeostasis, we also performed GTT and ITT. GTT revealed that Cre-injected mice had
217 consistently elevated glucose levels, indicative of higher glucose tolerance (**Fig. 1L**), while ITT
218 revealed that they had insulin resistance (**Fig. 1M**). These results indicate that Cre recombinase
219 expression in the PVN region of *Crh*$^{f/f}$ mice leads to obesity development and maintenance
220 through changes in food intake behavior and energy expenditure and causes metabolic
221 syndrome resembling type 2 diabetes mellitus.

222 Having observed the development of diabetes and obesity in the PVN Cre-injected *Crh*$^{f/f}$ mice,
223 we sought to validate these findings as attributable to the depletion of hypothalamic CRH. We
224 examined CRH expression using immunohistochemistry and found decreased CRH-positive cell
225 density in the PVN of AAV-Cre-injected mice (**Fig. 2A & 2C**). This suggested that CRH
226 expression was suppressed, which supports the hypothesis that PVN CRH participates in
227 regulating metabolism. However, this hypothesis is complicated by the observation of decreased
228 OXT expression in brain sections of the same animals with Cre injections (**Fig. 2B & 2D**).
229 Decreased expression of both CRH and OXT was accompanied with a trend toward reduced
230 cell density as measured by DAPI staining (**Fig. 2E**). Based on these data, we caution that
231 virally expressed Cre recombinase may be sufficient to deplete CRH from the PVN of *Crh*$^{f/f}$
232 animals but may also have an off-target impact on PVN neuronal cells.

233 ***Delivery of AAV-mediated Cre in the PVN rapidly alters behavior and causes metabolic***
234 ***syndrome in wild-type animals.***
235 While OXT expression may have decreased due to the development of obesity, the trend of
236 decreased cell density in the AAV-Cre group led us to hypothesize that the AAV-Cre virus may

237 impact PVN neuronal survival. The toxicity of Cre expression on cellular health has been
238 reported previously [13, 14, 29, 30].

239 To this end, we examined the impacts of AAV-Cre in C57BL/6 wild-type (WT) mice (**Fig. 3A**).
240 Similar to the AAV-Cre injected *Crh*$^{f/f}$ animals, we found a marked reduction in plasma
241 corticosterone levels in WT mice injected with AAV-Cre (**Fig. 3B**). They also gained significant
242 body weight potentially due to hyperphagia (**Fig. 3C-D**). Given that our observations closely
243 mirrored those found in *Crh*$^{f/f}$ mice, we also assessed changes in anxiety-like behaviors (**Fig.
244 S3A & S3C**). AAV-Cre-injected mice spent less time in the center zone during the open field test
245 (**Fig. S3B**). Consistent with this, Cre mice spent more time in the dark zone of the light-dark box
246 (**Fig. S3D**). These data suggest that the behavioral, metabolic, and cellular alterations observed
247 with Cre injection in the PVN may be due to the expression of the Cre-encoding viral vector.

248 We next systematically evaluated the number of neurons in the PVN of WT mice following AAV-
249 Cre or AAV-GFP injections using neuronal nuclei (NeuN) staining (**Fig. 3E**). Expression of NeuN
250 was significantly decreased across most of the PVN with the administration of AAV-Cre, likely
251 due to diffusion (**Fig. 3F**). Again, accompanied by the enlarged visual appearance of the third
252 ventricle, the widespread decline in neuronal density in AAV-Cre-expressing mice lends support
253 to the idea of toxic and nonspecific AAV-Cre action, resembling the effects of a chemical lesion
254 for PVN neuronal cells [31, 32]. This neuronal cell loss is accompanied by astrogliosis and
255 microglial cell activation (**Fig. 3G-I**).

256 Together, these data suggest that AAV-Cre injection may cause non-specific cell death at the
257 injection site, with PVN neuronal ablation causing obesity and diabetes. This is consistent with
258 previous reports that PVN lesions result in severe obesity and dysregulated metabolism [31, 32,
259 33, 34, 35].

260 ***Delivery of AAV-mediated Cre in the dorsal lateral septum induces neuronal cell lesions***
261 ***without causing metabolic syndrome in Glp1r*** $^{f/f}$ ***animals.***
262 To further confirm the apparent toxicity of the AAV-Cre that we used, we tested it in another
263 brain region: the dorsal lateral septum (dLS). The glucagon-like peptide-1 receptor (GLP-1R) is
264 highly expressed in dLS and is implicated in feeding and metabolism [36, 37, 38, 39]. We
265 assessed if a diluted AAV-Cre could be used to determine endogenous GLP-1R function. To
266 prevent the possibility of cellular toxicity due to high AAV titers, we diluted our AAV to 5 x 10^{12}
267 vg/mL and only injected 100 nL. We injected this AAV-Cre or a control vector in *Glp1r* $^{f/f}$ mouse

268 dLS (**Fig. S4A**), but we did not observe significant changes in body weight or metabolism within
269 4 weeks of injection (**Fig. S4B**). However, we found significantly decreased NeuN positive cell
270 density (**Fig. S4C-D**), suggesting that Cre viral vector injection in the mouse brain causes
271 neuronal cell loss.

272 ***Delivery of an alternative preparation of AAV-Cre in PVN avoids cell death and body***
273 ***weight changes in Crh$^{f/f}$ mice.***
274 We next tested if our findings were representative of all viral vectors delivering Cre
275 recombinase. We injected a preparation of AAV8-hSyn-Cre-GFP (UNC Vector Core) at the
276 provided titer (2.5 x 10^{12} vg/mL) in Crh$^{f/f}$ male mouse PVN (**Fig. 4A**). We found minimal changes
277 in body weight after 6 weeks of injection (**Fig. 4B**), suggesting that toxicity was attenuated.
278 Accordingly, we found no changes in neuronal cell density (**Fig. 4C-D, Fig. S5A&B**). Together,
279 these results point toward disparate and variable effects of AAV-Cre viruses, potentially due to
280 preparation or construction of the specific batch of viruses.

281 **Discussion**

282 In this study, we showed that delivery of one preparation of AAV-Cre recombinase in the PVN of
283 adult mice can lead to the development of metabolic syndrome and alterations in food-related
284 and anxiety-like behaviors, as well as metabolic phenotype. We demonstrated that *Crh$^{f/f}$* mice
285 expressing AAV-Cre in PVN develop obesity largely mediated by hyperphagia and changes in
286 energy expenditure. Moreover, this develops alongside glucose tolerance and insulin resistance,
287 as well as decreased locomotion. We investigated whether CRH was truly and specifically
288 depleted and found off-target effects on OXT expression (**Fig. 2**) and cell loss at sites of Cre
289 viral vector injections in either *Crh$^{f/f}$* or WT mice. These data suggested off-target effects of our
290 viral vector and indicate that caution should be used when interpreting the physiological
291 consequences of AAV injection in adult animals. Intriguingly, we found that another preparation
292 of AAV-Cre did not lead to lesions in PVN. Differences in how these viral vectors (batches, lots,
293 or other procedural variations) were constructed or prepared may potentially be the source of
294 this disparity. Variability in viral vector quality further accentuates the need to validate reagents
295 prior to experimental use.

296 Specific depletion of PVN-derived CRH has thus far not been shown to induce massive
297 metabolic dysregulation when knocked out using Cre expression driven by either *Crh$^{f/f}$* crossed
298 with *Sim1-Cre* mice or CRISPR [18, 40]. Our initial goal was to assess the impact of ablation of

299 PVN CRH in adult animals by using stereotactic injection of AAV-Cre. We observed massive
300 obesity and metabolic syndromes that starkly differ from other models of CRH signaling
301 deficiencies [18, 20, 40, 41, 42, 43]. CRH-deficient mice have intact feeding behavior, even after
302 stress [41]. Deletion of the type-1 CRH receptor yields conflicting results on food intake but
303 largely minimal effects on body weight [22, 44]. Global deletion of the type-2 receptor similarly
304 results in no changes in body weight despite significant increases in food consumption, likely
305 due to increased energy expenditure and sympathetic tone [45]. Despite the observation of
306 reduction of CRH expression and plasma corticosterone levels, which may be an indication of
307 impaired regulation of the hypothalamic-pituitary-adrenal axis (HPA), we surmise that any
308 metabolic or behavioral deficits reflected off-target effects of AAV-Cre. Indeed, we confirmed
309 that neuronal cell death and reactive gliosis occurred in the PVN with AAV-Cre expression,
310 resembling a response to central nervous system injury. Therefore, the study cannot conclude
311 whether adult ablation of CRH in the PVN leads to metabolic or behavioral changes in adult
312 animals. While we have preliminarily shown that an alternatively sourced AAV-Cre does not
313 cause significant body weight changes in *Crh*$^{f/f}$ mice, further behavioral and metabolic
314 phenotyping—as well as validation that CRH is fully knocked out—must be performed in future
315 studies to concretely resolve this aim.

316 The PVN is speculated to provide top-down control of feeding-related information processing via
317 intrahypothalamic connections or dense projections to midbrain and hindbrain regions [2].
318 These results could not provide insights on CRH impact on metabolism but highlight the
319 necessity of the PVN in regulating energy homeostasis and body weight. These findings are in
320 accord with prior ablation experiments and more recent work on genetic knockout models
321 specific to the PVN [31, 32]. It has been shown that unilateral PVN electrolytic lesions would
322 increase lipid accumulation in white adipose tissue ipsilateral to the side of the PVN [46].
323 Chronically inhibiting PVN MC4R/PDYN neuron synaptic release by expressing tetanus toxin or
324 ablating those neurons by expressing caspase-3 resulted in pronounced hyperphagia, obesity,
325 and a significant elevation in food consumption [32]. Our metabolic phenotyping data revealed
326 that cellular lesions of PVN develop a strong obesity phenotype largely mediated by
327 hyperphagia and changes in energy expenditure. Moreover, dysfunction of the PVN induces
328 hypersomnia and mediates the diurnal rhythm of metabolism in mice [47, 48]. Consistent with
329 this, we also found that changes in energy expenditure were more pronounced in AAV-Cre-
330 injected mice during dark cycles (**Fig. 1H**).

331 Manipulating gene expression on and off using AAVs in genetically engineered animals is one of
332 the most powerful tools to bypass transient developmental transcription for studying gene
333 function *in vivo* [8, 12]. For example, it has been shown that knockout of *Glp1r* via AAV-Cre in
334 PVN demonstrated a significant obesity phenotype, which was not observed in *Glp1r*$^{f/f}$ mice
335 cross with SIM1- or NKX2.1-Cre mice [8, 49]. Similarly, AAV-CRISPR–Cas9-mediated ablation
336 of leptin receptor in arcuate nucleus demonstrated that agouti-related peptide (AgRP) neurons
337 but not proopiomelanocortin (POMC) neurons are required for the primary action of leptin to
338 regulate both energy balance and glucose homeostasis [12]. The present results add to a
339 growing body of literature suggesting that toxicity occurs irrespective of serotype and brain
340 region, though a systematic comparison is lacking. While we show toxicity with one viral
341 preparation in this study, previous studies have reported varying levels of success with this AAV-
342 Cre and others [9, 13, 14, 48, 50]. In the mesolimbic reward system, it has been reported that
343 Cre expression in the ventral tegmental area and substantia nigra can induce toxicity associated
344 with perturbations of dopamine-related behaviors [13, 14]. Further work delineating different
345 viral preparations and optimal titers for neuronal manipulations will be needed. Inducible
346 systems of Cre expression, such as those using tamoxifen, offer an appealing alternative to
347 constitutively expressed Cre systems; however, administration of tamoxifen has also been
348 reported to lead to cytotoxicity and off-target effects [51].

349 Our data confirm that the PVN is an important brain region in the regulation of metabolism;
350 dysfunction of the PVN, such as via neuronal death, causes obesity and type 2 diabetes. We
351 also conclude that AAV-Cre vector toxicity ablates PVN neurons and results in a phenotype that
352 is not associated with the gene of interest. These results underscore the importance of rigorous
353 controls to ensure virus quality and fidelity of action. Caution must especially be exercised when
354 the observed phenotype closely matches that of lesions in the area of use. Ensuring that
355 expression in wild-type mice results in no observable changes or that neuronal cell densities are
356 unaltered (if they are not expected to be) are two such methods of validating that the AAV is not
357 toxic on its own. Together, viral vectors represent a class of worthwhile tools to manipulate the
358 nervous system; however, scientists must take care to ensure that the potential for toxicity in
359 commonly used AAVs is ruled out in experimental design and data interpretation.

360 **Future Directions**

361 In this study, we exclusively examined the impact of two batches of AAV-hSyn-Cre after injecting
362 into the hypothalamus. It remains to be determined if the neurotoxicity stems from the AAV's

363 preparation in the particular batch. Moreover, it is essential to understand the impact of AAV-Cre
364 on various glial cell types and neurons in different brain regions. Furthermore, the molecular
365 mechanisms behind the neurotoxic effects have not been explored in this study, warranting
366 future mechanistic research.
367

368 **Author contributions**

369 R.S. conducted animal behavior assays, histology, and data analysis. E.P. helped with histology
370 and imaging analysis. N.B. helped with histology and imaging analysis. Y.L. conducted
371 stereotactic surgeries, animal behavior analysis, and histology. H.J.K. conducted CLAMS
372 experiments and corresponding data analysis. L.W. conducted stereotactic surgeries. L.W. and
373 Z.P.P. conceived the project, and designed the experiments, and wrote the paper with R.S. with
374 input from all authors.

375 **Acknowledgments**
376 We thank Dr. Larry Zweifel of the University of Washington for providing us the $CRH^{flox/flox}$ mouse
377 line. This study was supported by grants from the Robert Wood Johnson Foundation to the
378 Child Health Institute of New Jersey (RWJF grant #74260), and the NIH NIDDK R01DK131452.
379 L.W. was supported by the New Jersey Governor's Council for Medical Research and Treatment
380 of Autism Postdoctoral Fellowship (CAUT24DFP005) and the NExT-Metabolism Pilot Award
381 (500301). R.S. was supported by Rutgers Aresty Research Center's independent research
382 award. The authors would like to thank Dr. Mark Rossi (Rutgers University) for critical reading of
383 the manuscript and insightful comments. The graphical abstract was created with BioRender.

384 **Data Availability**
385 The code used to analyze open-field test data can be found at
386 https://github.com/RohanSavani/OpenFieldAnalysis. The data from the current study are
387 available from the corresponding authors upon reasonable request.

388 **Supplementary Data**
389 Supplementary data to this article: Supplemental Figures S1-S4
390

391 **References**

392 1. Ferguson AV, Latchford KJ, Samson WK. The paraventricular nucleus of the
393 hypothalamus - a potential target for integrative treatment of autonomic dysfunction. Expert
394 Opin Ther Targets. 2008;12(6):717-27. https://doi.org/10.1517/14728222.12.6.717
395 2. Watts AG, Kanoski SE, Sanchez-Watts G, Langhans W. The physiological control of
396 eating: signals, neurons, and networks. Physiological Reviews. 2021;102(2):689-813.
397 https://doi.org/10.1152/physrev.00028.2020
398 3. Qin C, Li J, Tang K. The Paraventricular Nucleus of the Hypothalamus: Development,
399 Function, and Human Diseases. Endocrinology. 2018;159(9):3458-72.
400 https://doi.org/10.1210/en.2018-00453
401 4. Manaye KF, Lei DL, Tizabi Y, Dávila-García MI, Mouton PR, Kelly PH. Selective neuron
402 loss in the paraventricular nucleus of hypothalamus in patients suffering from major depression
403 and bipolar disorder. J Neuropathol Exp Neurol. 2005;64(3):224-9.
404 https://doi.org/10.1093/jnen/64.3.224
405 5. Benarroch EE. Paraventricular nucleus, stress response, and cardiovascular disease.
406 Clinical Autonomic Research. 2005;15(4):254-63. https://doi.org/10.1007/s10286-005-0290-7
407 6. Sauer B, Henderson N. Site-specific DNA recombination in mammalian cells by the Cre
408 recombinase of bacteriophage P1. Proceedings of the National Academy of Sciences.
409 1988;85(14):5166-70. https://doi.org/doi:10.1073/pnas.85.14.5166
410 7. Tsien JZ, Chen DF, Gerber D, Tom C, Mercer EH, Anderson DJ, et al. Subregion- and
411 Cell Type–Restricted Gene Knockout in Mouse Brain. Cell. 1996;87(7):1317-26.
412 https://doi.org/10.1016/S0092-8674(00)81826-7
413 8. Liu J, Conde K, Zhang P, Lilascharoen V, Xu Z, Lim BK, et al. Enhanced AMPA Receptor
414 Trafficking Mediates the Anorexigenic Effect of Endogenous Glucagon-like Peptide-1 in the
415 Paraventricular Hypothalamus. Neuron. 2017;96(4):897-909.e5.
416 https://doi.org/https://doi.org/10.1016/j.neuron.2017.09.042
417 9. Deng Y, Dickey JE, Saito K, Deng G, Singh U, Jiang J, et al. Elucidating the role of Rgs2
418 expression in the PVN for metabolic homeostasis in mice. Mol Metab. 2022;66:101622.
419 https://doi.org/10.1016/j.molmet.2022.101622
420 10. Souza LAC, Worker CJ, Li W, Trebak F, Watkins T, Gayban AJB, et al. (Pro)renin
421 receptor knockdown in the paraventricular nucleus of the hypothalamus attenuates hypertension
422 development and AT(1) receptor-mediated calcium events. Am J Physiol Heart Circ Physiol.
423 2019;316(6):H1389-h405. https://doi.org/10.1152/ajpheart.00780.2018
424 11. Xia H, de Queiroz TM, Sriramula S, Feng Y, Johnson T, Mungrue IN, et al. Brain ACE2
425 overexpression reduces DOCA-salt hypertension independently of endoplasmic reticulum
426 stress. Am J Physiol Regul Integr Comp Physiol. 2015;308(5):R370-8.
427 https://doi.org/10.1152/ajpregu.00366.2014
428 12. Xu J, Bartolome CL, Low CS, Yi X, Chien C-H, Wang P, et al. Genetic identification of
429 leptin neural circuits in energy and glucose homeostases. Nature. 2018;556(7702):505-9.
430 https://doi.org/10.1038/s41586-018-0049-7
431 13. Erben L, Welday JP, Murphy R, Buonanno A. Toxic and Phenotypic Effects of AAV_Cre
432 Used to Transduce Mesencephalic Dopaminergic Neurons. Int J Mol Sci. 2022;23(16).
433 https://doi.org/10.3390/ijms23169462
434 14. Rezai Amin S, Gruszczynski C, Guiard BP, Callebert J, Launay J-M, Louis F, et al. Viral
435 vector-mediated Cre recombinase expression in substantia nigra induces lesions of the
436 nigrostriatal pathway associated with perturbations of dopamine-related behaviors and
437 hallmarks of programmed cell death. Journal of Neurochemistry. 2019;150(3):330-40.
438 https://doi.org/https://doi.org/10.1111/jnc.14684

15. Kim J, Lee S, Fang Y-Y, Shin A, Park S, Hashikawa K, et al. Rapid, biphasic CRF neuronal responses encode positive and negative valence. Nature Neuroscience. 2019;22(4):576-85. https://doi.org/10.1038/s41593-019-0342-2
16. Yuan Y, Wu W, Chen M, Cai F, Fan C, Shen W, et al. Reward Inhibits Paraventricular CRH Neurons to Relieve Stress. Curr Biol. 2019;29(7):1243-51.e4. https://doi.org/10.1016/j.cub.2019.02.048
17. Zhu C, Xu Y, Jiang Z, Tian JB, Cassidy RM, Cai Z-L, et al. Disrupted hypothalamic CRH neuron responsiveness contributes to diet-induced obesity. EMBO reports. 2020;21(7):e49210. https://doi.org/https://doi.org/10.15252/embr.201949210
18. Zhang R, Asai M, Mahoney CE, Joachim M, Shen Y, Gunner G, et al. Loss of hypothalamic corticotropin-releasing hormone markedly reduces anxiety behaviors in mice. Molecular Psychiatry. 2017;22(5):733-44. https://doi.org/10.1038/mp.2016.136
19. Muglia LJ, Jenkins NA, Gilbert DJ, Copeland NG, Majzoub JA. Expression of the mouse corticotropin-releasing hormone gene in vivo and targeted inactivation in embryonic stem cells. J Clin Invest. 1994;93(5):2066-72. https://doi.org/10.1172/jci117201
20. Muglia L, Jacobson L, Dikkes P, Majzoub JA. Corticotropin-releasing hormone deficiency reveals major fetal but not adult glucocorticoid need. Nature. 1995;373(6513):427-32. https://doi.org/10.1038/373427a0
21. Jiang Z, Tong Q. Hypothalamic CRH neurons: A crossroad between stress and metabolism. Current Opinion in Endocrine and Metabolic Research. 2022;26:100384. https://doi.org/https://doi.org/10.1016/j.coemr.2022.100384
22. Bradbury MJ, McBurnie MI, Denton DA, Lee K-F, Vale WW. Modulation of Urocortin-Induced Hypophagia and Weight Loss by Corticotropin-Releasing Factor Receptor 1 Deficiency in Mice*. Endocrinology. 2000;141(8):2715-24. https://doi.org/10.1210/endo.141.8.7606
23. Sanford CA, Soden ME, Baird MA, Miller SM, Schulkin J, Palmiter RD, et al. A Central Amygdala CRF Circuit Facilitates Learning about Weak Threats. Neuron. 2017;93(1):164-78. https://doi.org/10.1016/j.neuron.2016.11.034
24. Sisley S, Gutierrez-Aguilar R, Scott M, D'Alessio DA, Sandoval DA, Seeley RJ. Neuronal GLP1R mediates liraglutide's anorectic but not glucose-lowering effect. The Journal of Clinical Investigation. 2014;124(6):2456-63. https://doi.org/10.1172/JCI72434
25. Nath T, Mathis A, Chen AC, Patel A, Bethge M, Mathis MW. Using DeepLabCut for 3D markerless pose estimation across species and behaviors. Nature Protocols. 2019;14(7):2152-76. https://doi.org/10.1038/s41596-019-0176-0
26. Daviu N, Bruchas MR, Moghaddam B, Sandi C, Beyeler A. Neurobiological links between stress and anxiety. Neurobiology of Stress. 2019;11:100191. https://doi.org/https://doi.org/10.1016/j.ynstr.2019.100191
27. Sterley T-L, Baimoukhametova D, Füzesi T, Zurek AA, Daviu N, Rasiah NP, et al. Social transmission and buffering of synaptic changes after stress. Nature Neuroscience. 2018;21(3):393-403. https://doi.org/10.1038/s41593-017-0044-6
28. Füzesi T, Daviu N, Wamsteeker Cusulin JI, Bonin RP, Bains JS. Hypothalamic CRH neurons orchestrate complex behaviours after stress. Nat Commun. 2016;7:11937. https://doi.org/10.1038/ncomms11937
29. Semprini S, Troup TJ, Kotelevtseva N, King K, Davis JR, Mullins LJ, et al. Cryptic loxP sites in mammalian genomes: genome-wide distribution and relevance for the efficiency of BAC/PAC recombineering techniques. Nucleic Acids Res. 2007;35(5):1402-10. https://doi.org/10.1093/nar/gkl1108
30. Correa-da-Silva F, Kalsbeek MJ, Gadella FS, Oppersma J, Jiang W, Wolff SEC, et al. Reduction of oxytocin-containing neurons and enhanced glymphatic activity in the hypothalamic paraventricular nucleus of patients with type 2 diabetes mellitus. Acta Neuropathologica Communications. 2023;11(1):107. https://doi.org/10.1186/s40478-023-01606-w

31. Sims JS, Lorden JF. Effect of paraventricular nucleus lesions on body weight, food intake and insulin levels. Behavioural Brain Research. 1986;22(3):265-81. https://doi.org/https://doi.org/10.1016/0166-4328(86)90071-9
32. Li MM, Madara JC, Steger JS, Krashes MJ, Balthasar N, Campbell JN, et al. The Paraventricular Hypothalamus Regulates Satiety and Prevents Obesity via Two Genetically Distinct Circuits. Neuron. 2019;102(3):653-67.e6. https://doi.org/10.1016/j.neuron.2019.02.028
33. Leibowitz SF, Hammer NJ, Chang K. Hypothalamic paraventricular nucleus lesions produce overeating and obesity in the rat. Physiology & Behavior. 1981;27(6):1031-40. https://doi.org/https://doi.org/10.1016/0031-9384(81)90366-8
34. Fukushima M, Tokunaga K, Lupien J, Kemnitz JW, Bray GA. Dynamic and static phases of obesity following lesions in PVN and VMH. American Journal of Physiology-Regulatory, Integrative and Comparative Physiology. 1987;253(3):R523-R9. https://doi.org/10.1152/ajpregu.1987.253.3.R523
35. Gold RM, Jones AP, Sawchenko PE, Kapatos G. Paraventricular area: Critical focus of a longitudinal neurocircuitry mediating food intake. Physiology & Behavior. 1977;18(6):1111-9. https://doi.org/https://doi.org/10.1016/0031-9384(77)90019-1
36. Terrill SJ, Jackson CM, Greene HE, Lilly N, Maske CB, Vallejo S, et al. Role of lateral septum glucagon-like peptide 1 receptors in food intake. Am J Physiol Regul Integr Comp Physiol. 2016;311(1):R124-32. https://doi.org/10.1152/ajpregu.00460.2015
37. Rizzi-Wise CA, Wang DV. Putting Together Pieces of the Lateral Septum: Multifaceted Functions and Its Neural Pathways. eNeuro. 2021;8(6). https://doi.org/10.1523/eneuro.0315-21.2021
38. Bales MB, Centanni SW, Luchsinger JR, Fathi P, Biddinger JE, Le TDV, et al. High fat diet blunts stress-induced hypophagia and activation of Glp1r dorsal lateral septum neurons in male but not in female mice. Molecular Metabolism. 2022;64:101571. https://doi.org/https://doi.org/10.1016/j.molmet.2022.101571
39. Terrill SJ, Holt MK, Maske CB, Abrams N, Reimann F, Trapp S, et al. Endogenous GLP-1 in lateral septum promotes satiety and suppresses motivation for food in mice. Physiology & Behavior. 2019;206:191-9. https://doi.org/https://doi.org/10.1016/j.physbeh.2019.04.008
40. Li S-B, Borniger JC, Yamaguchi H, Hédou J, Gaudilliere B, de Lecea L. Hypothalamic circuitry underlying stress-induced insomnia and peripheral immunosuppression. Science Advances.6(37):eabc2590. https://doi.org/10.1126/sciadv.abc2590
41. Weninger SC, Muglia LJ, Jacobson L, Majzoub JA. CRH-deficient mice have a normal anorectic response to chronic stress. Regul Pept. 1999;84(1-3):69-74. https://doi.org/10.1016/s0167-0115(99)00070-1
42. Weninger SC, Dunn AJ, Muglia LJ, Dikkes P, Miczek KA, Swiergiel AH, et al. Stress-induced behaviors require the corticotropin-releasing hormone (CRH) receptor, but not CRH. Proceedings of the National Academy of Sciences. 1999;96(14):8283-8. https://doi.org/10.1073/pnas.96.14.8283
43. Dunn AJ, Swiergiel AH. Behavioral responses to stress are intact in CRF-deficient mice. Brain Research. 1999;845(1):14-20. https://doi.org/https://doi.org/10.1016/S0006-8993(99)01912-5
44. Sakamoto R, Matsubara E, Nomura M, Wang L, Kawahara Y, Yanase T, et al. Roles for corticotropin-releasing factor receptor type 1 in energy homeostasis in mice. Metabolism. 2013;62(12):1739-48. https://doi.org/https://doi.org/10.1016/j.metabol.2013.08.005
45. Bale TL, Anderson KR, Roberts AJ, Lee K-F, Nagy TR, Vale WW. Corticotropin-Releasing Factor Receptor-2-Deficient Mice Display Abnormal Homeostatic Responses to Challenges of Increased Dietary Fat and Cold. Endocrinology. 2003;144(6):2580-7. https://doi.org/10.1210/en.2002-0091

538 46. Foster MT, Song CK, Bartness TJ. Hypothalamic paraventricular nucleus lesion
539 involvement in the sympathetic control of lipid mobilization. Obesity (Silver Spring).
540 2010;18(4):682-9. https://doi.org/10.1038/oby.2009.345
541 47. Chen CR, Zhong YH, Jiang S, Xu W, Xiao L, Wang Z, et al. Dysfunctions of the
542 paraventricular hypothalamic nucleus induce hypersomnia in mice. Elife. 2021;10.
543 https://doi.org/10.7554/eLife.69909
544 48. Kim ER, Xu Y, Cassidy RM, Lu Y, Yang Y, Tian J, et al. Paraventricular hypothalamus
545 mediates diurnal rhythm of metabolism. Nat Commun. 2020;11(1):3794.
546 https://doi.org/10.1038/s41467-020-17578-7
547 49. Burmeister MA, Ayala JE, Smouse H, Landivar-Rocha A, Brown JD, Drucker DJ, et al.
548 The Hypothalamic Glucagon-Like Peptide 1 Receptor Is Sufficient but Not Necessary for the
549 Regulation of Energy Balance and Glucose Homeostasis in Mice. Diabetes. 2017;66(2):372-84.
550 https://doi.org/10.2337/db16-1102
551 50. Bozadjieva-Kramer N, Ross RA, Johnson DQ, Fenselau H, Haggerty DL, Atwood B, et
552 al. The Role of Mediobasal Hypothalamic PACAP in the Control of Body Weight and
553 Metabolism. Endocrinology. 2021;162(4). https://doi.org/10.1210/endocr/bqab012
554 51. Lee CM, Zhou L, Liu J, Shi J, Geng Y, Liu M, et al. Single-cell RNA-seq analysis
555 revealed long-lasting adverse effects of tamoxifen on neurogenesis in prenatal and adult brains.
556 Proc Natl Acad Sci U S A. 2020;117(32):19578-89. https://doi.org/10.1073/pnas.1918883117
557

558 **Figures and Figure Legends**

559 **Figure 1. AAV-Cre administration in PVN of male *Crh*$^{f/f}$ mice results in the development of**
560 **metabolic syndrome. (A)** Experimental paradigm for virus delivery. AAV-Cre or AAV-eGFP was
561 stereotactically injected into the adult male murine PVN. **(B)** Plasma corticosterone decreased
562 following AAV-Cre injection ($t(12) = 4.011$, $p = 0.0017$). **(C)** Changes in body weight following
563 virus delivery at week 0 (two-way ANOVA, main effect of Group: $F(1, 12) = 294.1$, $p < 0.0001$;
564 main effect of Time: $F(1.378, 16.53) = 228.5$, $p < 0.0001$; interaction between Group and Time:
565 $F(9, 108) = 138.4$, $p < 0.0001$). **(D)** Daily chow intake following virus injection increased with
566 AAV-Cre ($t(12) = 3.152$, $p = 0.0083$). **(E)** Changes in oxygen consumption were observed over
567 the course of 96 hours. **(F)** Quantification of the decrease in oxygen consumption in AAV-Cre-
568 injected mice (two-way ANOVA with Bonferroni's multiple comparisons test, main effect of
569 Group: $F(1, 12) = 25.11$, $p = 0.0003$; main effect of Time: $F(1, 12) = 208.4$, $p < 0.0001$;
570 interaction between Group and Time: $F(1, 12) = 43.58$, $p < 0.001$). **(G)** The respiratory
571 exchange ratio (RER) was unaltered (two-way ANOVA, no main effect of Group: $F(1, 12) =$
572 0.02021, $p = 0.8893$; no main effect of Time: $F(1, 12) = 2.970$, $p = 0.1105$; no interaction
573 between Group and Time: $F(1, 12) = 3.566$, $p = 0.0834$). **(H)** Energy expenditure decreased
574 following AAV-Cre delivery (two-way ANOVA with Bonferroni's multiple comparisons test, main
575 effect of Group: $F(1, 12) = 26.31$, $p = 0.0002$; main effect of Time: $F(1, 12) = 207.9$, $p < 0.0001$;
576 interaction between Group and Time: $F(1, 12) = 45.10$, $p < 0.0001$). **(I)** Locomotion in the x-axis
577 in the CLAMS cage decreased during the dark cycle (two-way ANOVA with Bonferroni's multiple
578 comparisons test, main effect of Group: $F(1, 12) = 8.461$, $p = 0.0131$; main effect of Time: $F(1,$
579 $12) = 41.86$, $p < 0.0001$, interaction between Group and Time: $F(1, 12) = 10.17$, $p = 0.0078$). **(J)**
580 Proportion of fat mass as determined by EchoMRI increased in AAV-Cre-injected mice ($t(12) =$
581 12.67, $p < 0.0001$). **(K)** Changes in average blood glucose after overnight fasting ($t(12) = 5.888$,
582 $p < 0.0001$). **(L)** The glucose tolerance test reveals increased baseline blood glucose levels
583 (two-way ANOVA with Bonferroni's multiple comparisons test, main effect of Group: $F(1, 12) =$
584 22.30, $p = 0.0005$; main effect of Time: $F(2.717, 32.60) = 24.72$, $p < 0.0001$; interaction
585 between Group and Time: $F(4, 48) = 3.111$, $p = 0.0235$). **(M)** The insulin tolerance test reveals
586 insulin tolerance (two-way ANOVA with Bonferroni's multiple comparisons test, main effect of
587 Group: $F(1, 11) = 11.30$, $p = 0.0063$; main effect of Time: $F(1.712, 18.84) = 55.72$, $p < 0.0001$;
588 no interaction between Group and Time: $F(2, 22) = 0.6622$, $p = 0.5257$). Sample sizes are as
589 shown on graphs (n = 7 mice per group). Data are presented as individual points and mean ± or
590 + SEM.

591 **Figure 2. AAV-Cre action in PVN of *Crh*$^{f/f}$ mice depletes CRH and OXT. (A)** Example
592 comparison of CRH expression in PVN between both groups. **(B)** Example of OXT expression
593 in PVN. **(C)** CRH-positive cell density decreased following AAV-Cre expression in *Crh*$^{f/f}$ PVN (t
594 (4) = 3.176, p = 0.0337). **(D)** OXT-positive cell density decreased as well (t (4) = 2.807, p =
595 0.0236). **(E)** Overall cell density trended toward a decline (t (4) = 2.511, p = 0.0660). Sample
596 sizes are as shown on graphs (n = 3 mice per group). Data are presented as individual points
597 and mean + SEM.

598 **Figure 3: AAV-Cre action in wild-type PVN induces metabolic changes, neuronal cell**
599 **death, and recruitment of glia. (A)** Experimental paradigm for virus delivery in wild-type male
600 mice. **(B)** Plasma corticosterone levels decreased after AAV-Cre injection (t (7) = 3.260, p =
601 0.0139). **(C)** Body weight changes followed virus delivery (two-way ANOVA, main effect of
602 Group: F (1, 7) = 22.37, p = 0.0021; main effect of Time: F (1.134, 7.940) = 191.5, p < 0.0001;
603 interaction between Group and Time: F (6, 42) = 79.71, p < 0.0001). **(D)** Daily food intake
604 increased in AAV-Cre-injected mice (Mann-Whitney test, U = 0, p = 0.0159). **(E)** Example
605 images of neuronal nuclei (NeuN) across the PVN following injection in wild-type mice. **(F)**
606 Quantification of neuron density at different stereotactic coordinates: -0.34 (t (5) = 18.72, p <
607 0.0001), -0.58 (t (5) = 5.343, p = 0.0031), -0.94 (t (5) = 3.053, p = 0.0283), and -1.22 (t (5) =
608 3.372, p = 0.0199). **(G)** Example comparison of glial fibrillary acidic protein (GFAP) and ionized
609 calcium binding adaptor molecule 1 (Iba1) expression in the wild-type PVN between the two
610 groups. **(H)** Expression of astrocytes increased as quantified by GFAP fluorescence area (t (6) =
611 3.017, p = 0.0235) **(I)** Expression of microglia increased as quantified by Iba1 fluorescence area
612 (t (6) = 2.917, p = 0.0267). Sample sizes are as shown on graph: **(F)** n = 3 control, 4 AAV-Cre
613 **(H, I)** n = 4 per group. Data are presented as individual points and mean ± or + SEM.

614 **Figure 4: An alternative preparation of AAV-Cre does not lead to cell death in PVN. (A)**
615 Experimental paradigm for virus delivery in male *Crh-flox* mice. (B) Body weight does not
616 change following delivery (two-way ANOVA, main effect of Group: F (1, 7) = 5.304, p = 0.0547;
617 main effect of Time: F (6, 42) = 19.71, p < 0.0001; interaction between Group and Time: F (6,
618 42) = 1.729, p = 0.1379). **(C)** Example images of NeuN density in PVN following injection. **(D)**
619 Neuron density did not change following AAV-Cre injection (t (5) = 0.1005, p = 0.9238). Data are
620 presented as individual points and mean ± or + SEM.

621

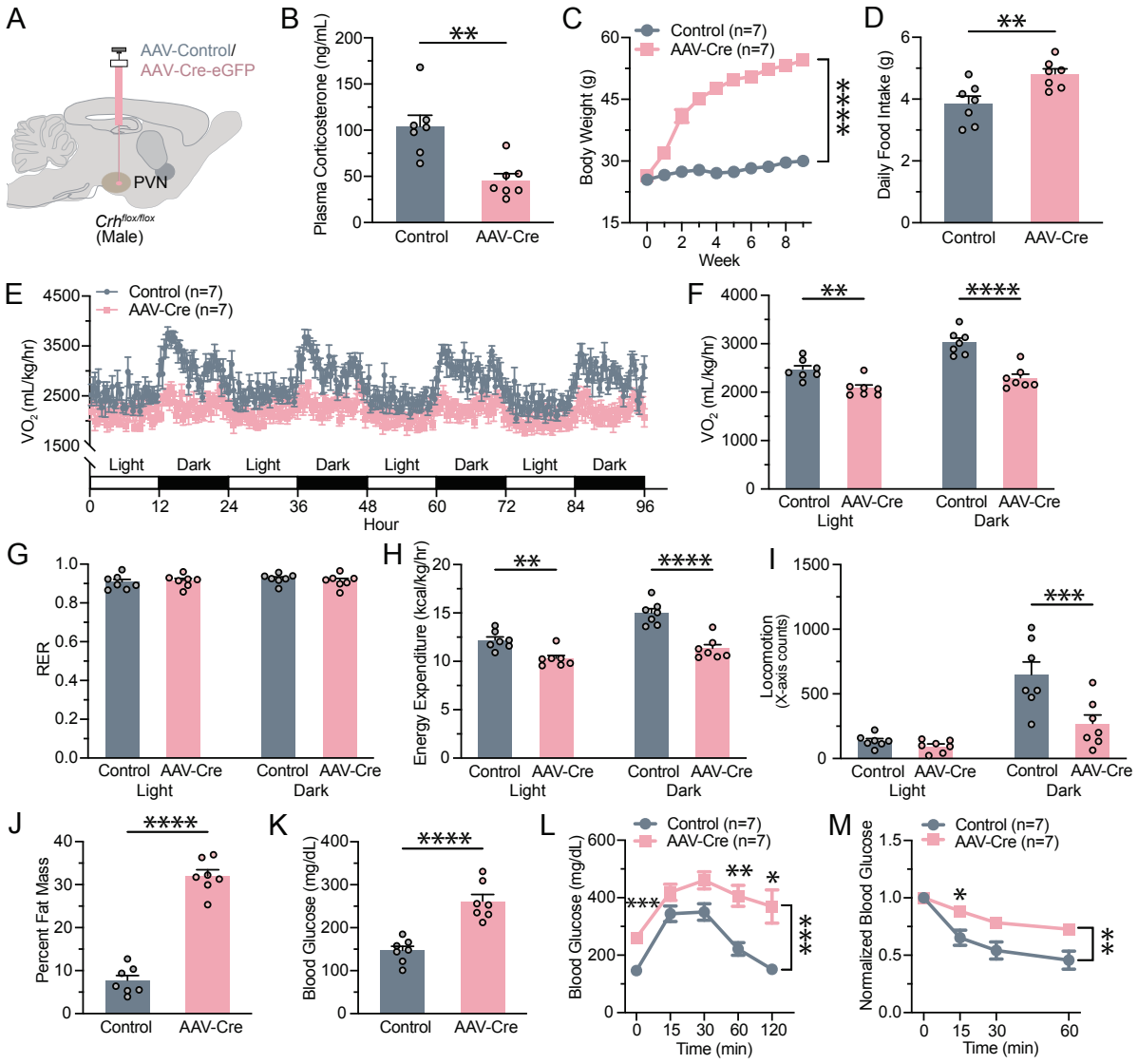

Savani et al. Figure 1

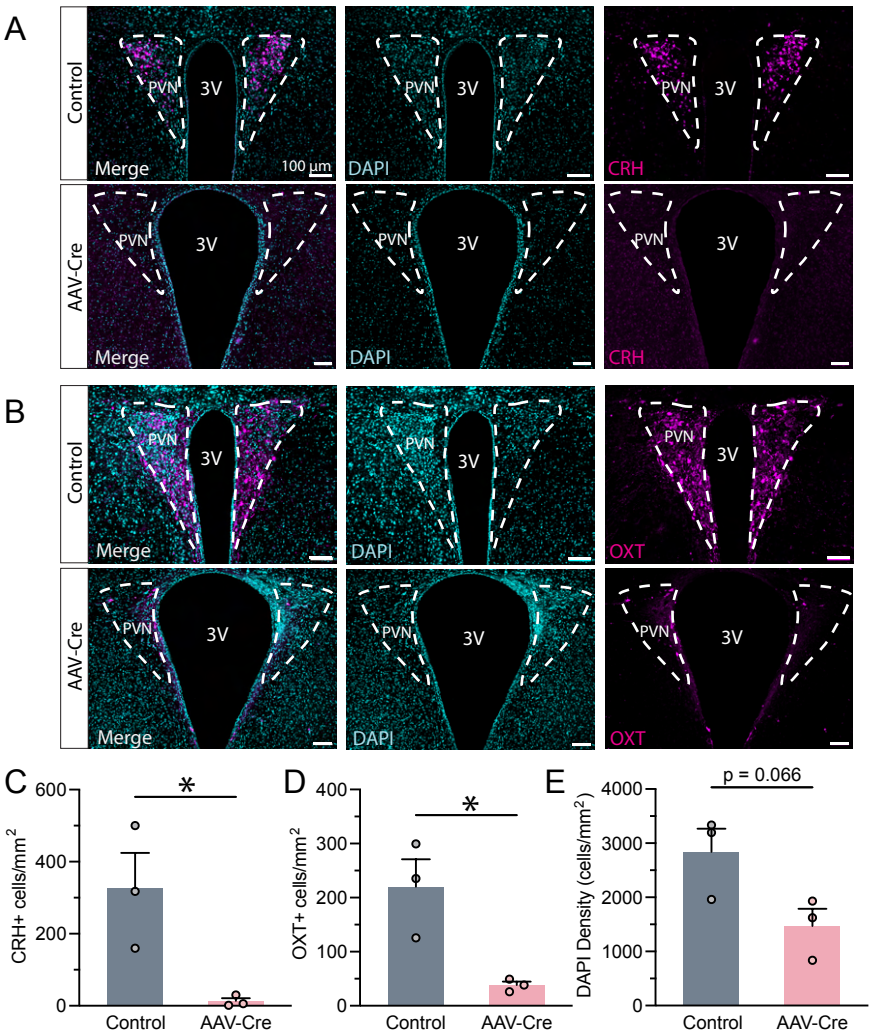

Savani et al. Figure 2

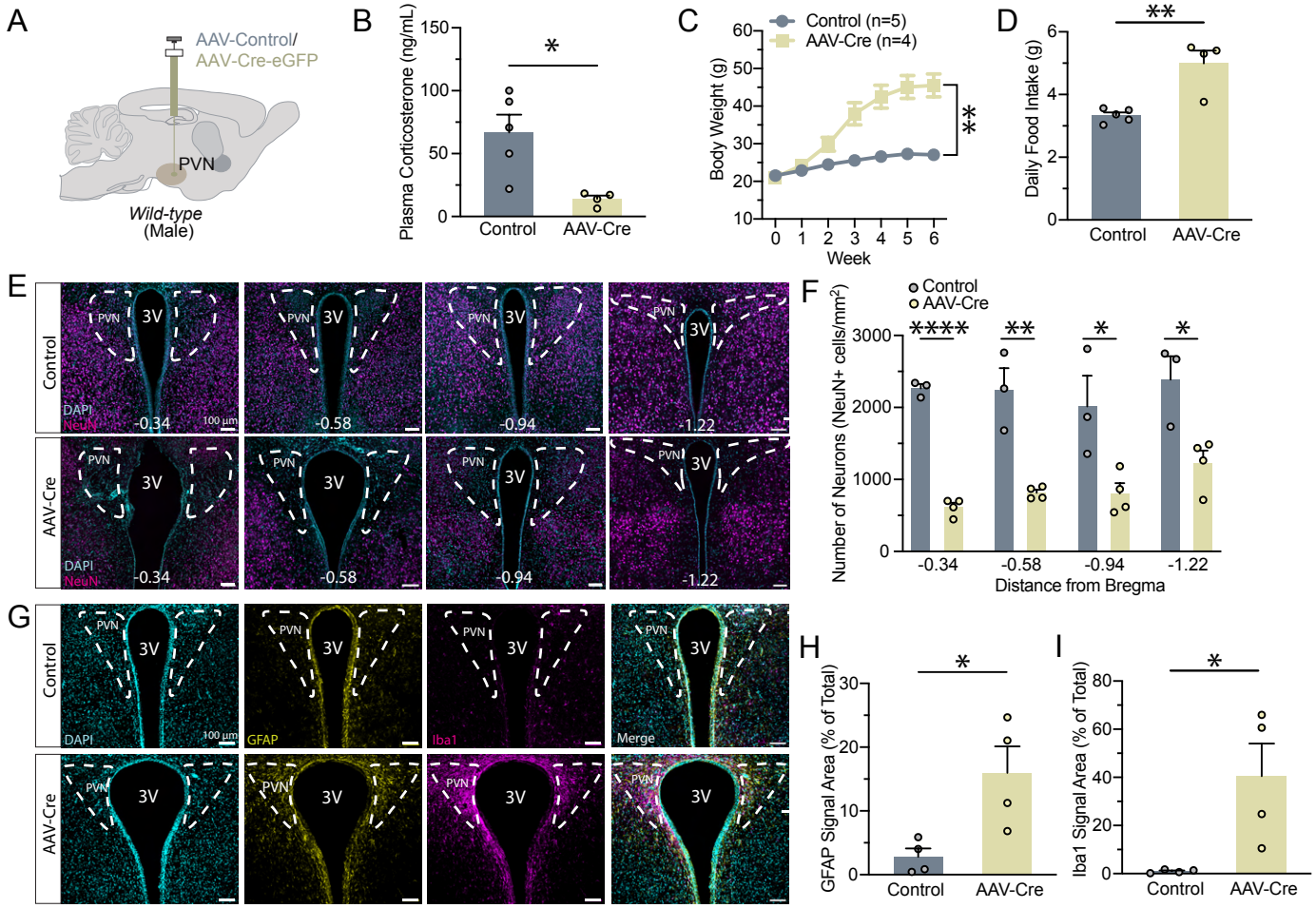

Savani et al. Figure 3

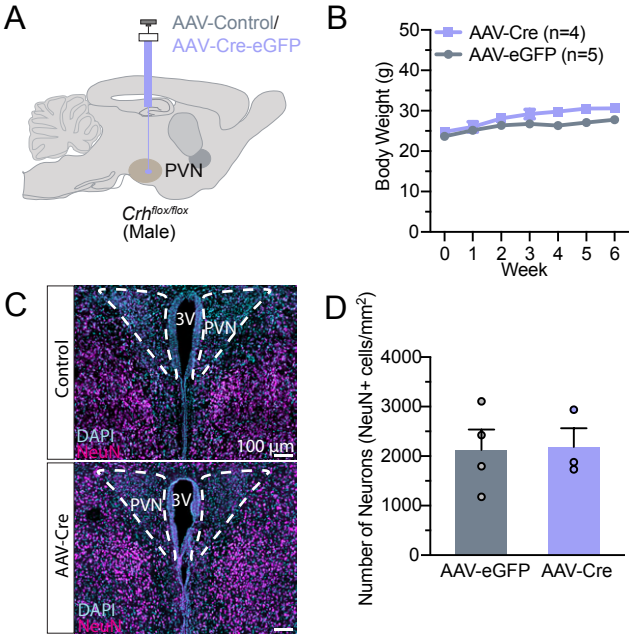

Savani et al. Figure 4

Supplementary Information

Metabolic and behavioral alterations associated with viral vector-mediated toxicity in the paraventricular hypothalamic nucleus

Rohan Savani[1,2], Erin Park[1,2], Nidhi Busannagari[1,2], Yi Lu[1], Hyokjoon Kwon[3], Le Wang[1, *], Zhiping P. Pang[1, *]

[1]The Child Health Institute of New Jersey, Robert Wood Johnson Medical School, Rutgers, The State University of New Jersey, New Brunswick, NJ, USA

[2]Department of Cell Biology and Neuroscience, Undergraduate Program, Rutgers, The State University of New Jersey, New Brunswick, NJ, USA

[3]Department of Medicine, Rutgers-Robert Wood Johnson Medical School, New Brunswick, NJ, 08901, USA

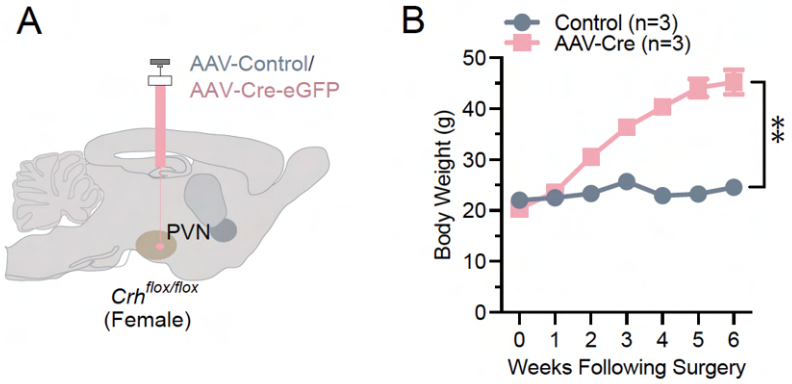

Figure S1: AAV-Cre expression in the PVN of female *Crh*$^{f/f}$ mice recapitulates body weight increases. (A) Experimental paradigm for virus delivery. **(B)** Body weight increases following AAV-Cre injection (two-way ANOVA, main effect of Group: $F(1, 4) = 59.08$, $p = 0.0015$; main effect of Time: $F(1.782, 7.129) = 77.74$, $p < 0.0001$; interaction between Group and Time: $F(6, 24) = 58.41$, $p < 0.0001$). Sample sizes are as shown on graphs (n = 3 mice per group). Data are presented as mean ± SEM.

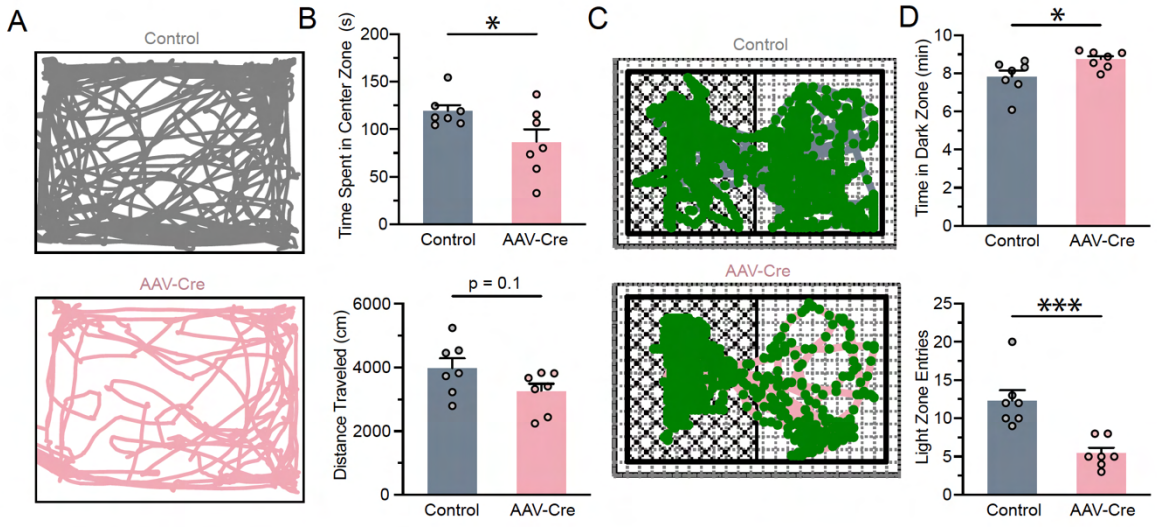

Figure S2: *Crh*$^{f/f}$ mice expressing AAV-Cre in PVN display elevated anxiety-like behaviors. **(A)** Representative trajectories of AAV-GFP- (top) and AAV-Cre-injected (bottom) male mice during the open field test. **(B)** AAV-Cre-injected mice spent less time in the center zone of the open field test ($t(12) = 2.181$, $p = 0.0498$), and changes in distance traveled were not significant ($t(12) = 1.811$, $p = 0.0952$) during the open field test. **(C)** Representative trajectories of both groups during the light-dark box test. **(D)** Time spent in the dark zone increased ($t(12) = 2.416$, $p = 0.0326$), and entries into the light zone decreased (Mann-Whitney test, $U = 0$, $p = 0.0006$) during the light-dark box test. Sample sizes are as shown on graphs (n = 7 mice per group). Data are presented as individual points and mean + SEM.

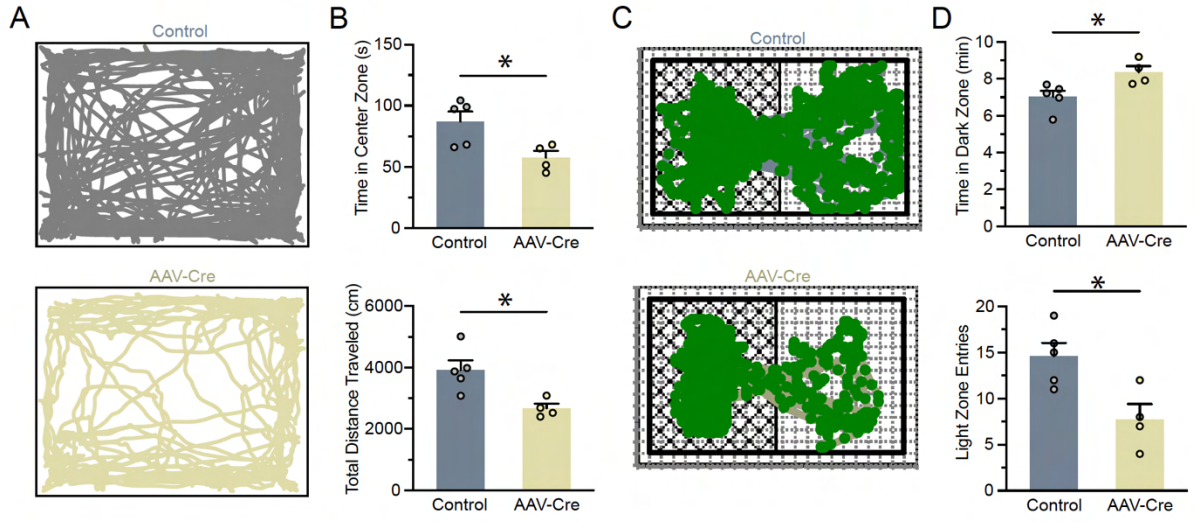

Figure S3. Wild-type male mice injected with AAV-Cre in PVN exhibit increased anxiety-like behaviors. (A) Representative traces of wild-type mice during the open field test. **(B)** During the open field test, time spent in the center zone decreased ($t(7) = 2.817$, $p = 0.0259$), and total distance traveled decreased ($t(7) = 3.275$, $p = 0.0136$). **(C)** Representative movement during the light-dark box test for both groups. **(D)** During the light-dark box test, time spent in the dark zone increased ($t(7) = 2.798$, $p = 0.0266$), and entries into the light zone decreased ($t(7) = 3.142$, $p = 0.0163$). Sample sizes are as shown on graphs (n = 5 AAV-GFP-injected mice, n = 4 AAV-Cre-injected mice). Data are presented as individual points and mean + SEM.

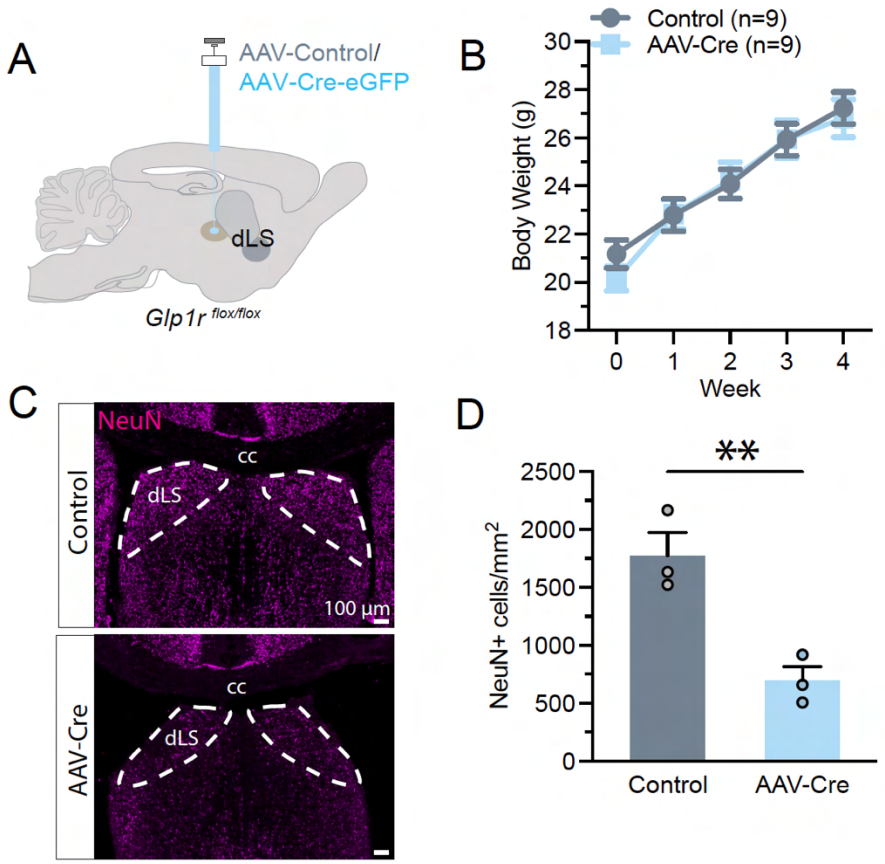

Figure S4. AAV-Cre expression in the dLS of male *Glp1r*$^{f/f}$ mice results in cell death without metabolic deficits. (A) Experimental paradigm for virus delivery. **(B)** Body weight was unchanged (two-way ANOVA, main effect of Group: F (1, 16) = 0.07282, p = 0.7907; main effect of Time: F (1.826, 29.22) = 364.6, p < 0.0001; interaction between Group and Time: F (4, 64) = 3.406, p = 0.0138). **(C)** Representative images of neuronal nuclei in the dLS after AAV-GFP or AAV-Cre injection. **(D)** Neuron density decreased in the dLS after AAV-Cre expression (t (4) = 4.631, p = 0.0098). Sample sizes are as shown on graphs: **(B)** n = 9 mice per group; **(D)** n = 3 mice per group. Data are presented as individual points and mean ± or + SEM. cc: corpus callosum.

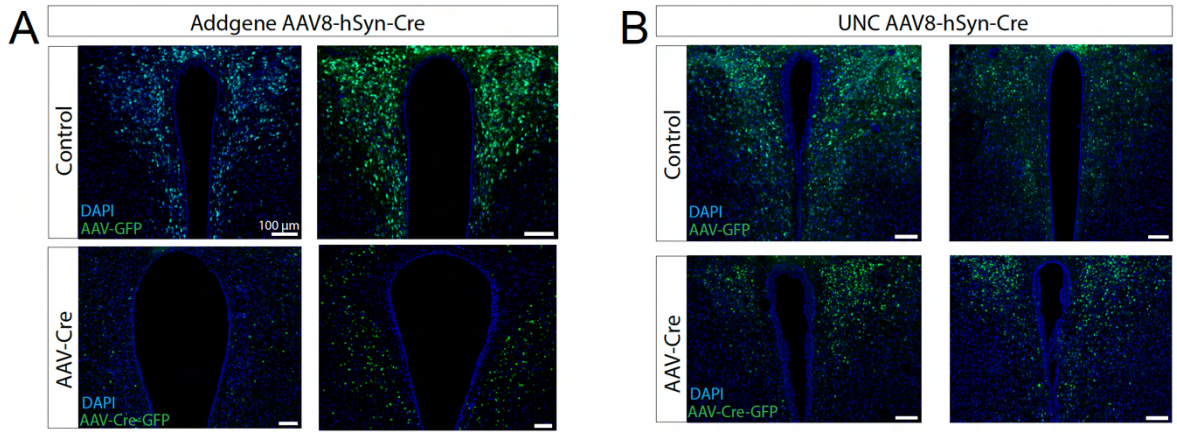

Figure S5: AAV-Cre-GFP Expression with AAV-Cre and AAV-GFP in PVN. (A) Examples of expression of AAV-GFP (control) or AAV-Cre-GFP in *Crh-flox* mice correspond to Figure 2. **(B)** Examples of expression in *Crh-flox* mice injected with the UNC Vector Core-sourced AAV-Cre correspond to Figure 4.